JAMES | Journal of Advances in Modeling Earth Systems

RESEARCH ARTICLE
10.1029/2019MS001686

A Steady-State Model for the Relationship Between Humidity, Instability, and Precipitation in the Tropics

Martin S. Singh[1,2], **Robert A. Warren**[1,2], **and Christian Jakob**[1,2]

[1]School of Earth, Atmosphere & Environment, Monash University, Clayton, Victoria, Australia, [2]Centre of Excellence for Climate Extremes, Monash University, Clayton, Victoria, Australia

Key Points:
- We derive a simple steady-state bulk-plume model for the temperature and humidity profiles of the atmosphere given the large-scale flow
- Bulk-plume model predicts increasing relative humidity and stability with increasing large-scale upward motion
- Bulk-plume model provides insight toward understanding relationships between convection and the large-scale environment at long time scales

Correspondence to:
Martin S. Singh,
martin.singh@monash.edu

Citation:
Singh, M. S., Warren, R. A., Jakob, C. (2019). A steady-state model for the relationship between humidity, instability, and precipitation in the tropics. *Journal of Advances in Modeling Earth Systems*, *11*. https://doi.org/10.1029/2019MS001686

Received 14 MAR 2019
Accepted 28 OCT 2019
Accepted article online 6 NOV 2019

Abstract A simple steady-state model for the thermodynamic structure of a convecting atmosphere under the influence of large-scale dynamics is derived based on a bulk-plume representation of convection. Given profiles of the large-scale vertical velocity and convective mass flux, the model predicts the steady-state temperature and environmental relative humidity profiles as a function of the convective entrainment rate and a parameter representing the importance of condensate reevaporation. The bulk-plume model determines the environmental relative humidity through a balance between the moistening effect of convective detrainment and the drying effect of subsidence in the cloud environment. As the convective mass flux is increased, the importance of detrainment moistening increases, leading to a higher environmental relative humidity. Since the precipitation rate also increases with the convective mass flux, this leads to a steady state in which the precipitation is a strongly increasing function of environmental relative humidity. The bulk-plume model also predicts that the atmospheric stability increases with large-scale upward motion, with the tropospheric lapse rate being most unstable under large-scale descent, when the environmental relative humidity is low. The above relationships are reproduced in a set of simulations with a cloud-system resolving model (CRM) run to equilibrium with imposed large-scale vertical velocity profiles. The results provide insight to the steady-state limit of the well-known problem of determining the relationships between large-scale conditions and the convective state of the atmosphere.

1. Introduction

One of the most important and long-standing problems in atmospheric science is the question of how convective-scale processes within the atmosphere influence, and are influenced by, the large-scale circulation. This question lies at the heart of our conceptual understanding of tropical circulations (Emanuel et al., 1994), and its answer is central to developing accurate parameterizations of convection for general circulation models. Such parameterizations will likely continue to be needed as part of our model hierarchy for many decades, notwithstanding the anticipated rise of global cloud-system resolving simulations for weather and climate studies.

A starting point for developing a complete theory for the interaction between convection and the large-scale flow is to understand the observed relationships between convective activity (i.e., precipitation) and the large-scale thermodynamic environment. For example, it is well known that, at a variety of different time scales, there is a strong and nonlinear relationship between the precipitation rate averaged over a mesoscale region and the total column water vapor (CWV) over both tropical oceans (e.g., Bretherton et al., 2004; Peters & Neelin, 2006; Rushley et al., 2018) and land (Schiro et al., 2016). Identifying the causes of this strong relationship is challenging because of the two-way nature of water vapor-convection interactions. Moist convection is known to be sensitive to environmental humidity, both through the influence of boundary-layer humidity on convective instability (Muller et al., 2009) and through the influence of free-tropospheric humidity on convective development, either directly through convective entrainment (e.g., Derbyshire et al., 2004) or indirectly through changes in stability driven by evaporation of precipitation (Virman et al., 2018). On the other hand, convection itself is known to play an important role in modulating tropospheric humidity (e.g., Thayer-Calder & Randall, 2009), and the moistening effects of convection on its environment may

also contribute to the observed precipitation-humidity relationship (Holloway & Neelin, 2009; Schiro et al., 2016).

At convective time scales, a number of lines of evidence point to a substantial role for convective entrainment in determining the precipitation-humidity relationship. For example, studies using entraining plume models have shown that the observed rapid increase of precipitation with CWV is consistent with a transition to positive plume buoyancy, provided the lower-tropospheric entrainment rate within the plume model is sufficiently large (Ahmed & Neelin, 2018; Sahany et al., 2012; Schiro et al., 2018). Furthermore, by varying the convective entrainment rate in a general circulation model, Kuo et al. (2017) showed that the effect of entrainment is central to the sharpness of the simulated precipitation-humidity relationship.

At time scales longer than a few hours, the temporally averaged precipitation rate is still a strong function of CWV, but the relationship is smoother than the case for near-instantaneous data (Kuo et al., 2018). For circulations that evolve slowly compared to convective processes, the moisture and energy budgets place additional constraints on the precipitation rate (Neelin & Held, 1987), and the importance of entrainment is less clear. For example, Emanuel (2019) used the vertically integrated moist static energy budget to show that a strong relationship between precipitation and column humidity for such "slow" circulations can arise independently of assumptions about entrainment. Determining to what extent such a model can account for the observed relationships between convection and its environment and on what time scales it may be valid requires careful quantitative comparison to observations.

In contrast to the precipitation-humidity relationship, the statistical relationship between precipitation and stability is less well known. The studies of deep convective onset cited above suggest that, at short (convective) time scales, precipitation is a strongly increasing function of conditional instability, provided the measure of conditional instability takes into account the effect of entrainment on convective clouds (Ahmed & Neelin, 2018; Schiro et al., 2018). However, at longer time scales, one might expect such instability to be removed by convection itself (e.g., Emanuel et al., 1994). Indeed, early studies suggested that the lapse rate in convecting regions of the tropics could not be distinguished from that of a moist adiabat (Xu & Emanuel, 1989). But more recent work indicates that tropical convective available potential energy (CAPE) peaks when the area fraction of convective precipitation is low (Davies et al., 2013) and in regions of the atmosphere that are relatively dry (Singh et al., 2017). Furthermore, the most intense thunderstorms, as measured by radar echo-top height, do not correspond to those storms with the largest local precipitation rates (Hamada et al., 2015), and they tend to occur in the convective margins rather than in regions of high mean precipitation (Zipser et al., 2006). Together, these studies point toward an inverse relationship between instability (as measured by, e.g., CAPE) and the area-averaged precipitation rate, at least over part of the precipitation distribution, and for time scales that are long compared to an individual convective event.

In this paper, we seek to understand relationships between convection and its thermodynamic environment at time scales long compared to the time scale over which the atmosphere is moistened by convection. In particular, we construct a simple model for the relationship between humidity, instability, and precipitation under steady-state conditions as a first step toward understanding these relationships in Earth's tropics. Previous studies have derived similar models that relate climatological precipitation to boundary conditions, such as the sea surface temperature or surface fluxes, using the vertically integrated moist static energy budget (e.g., Neelin & Held, 1987; Emanuel, 2019). Here, we take a simpler approach by considering the response of convection to an imposed large-scale flow. But rather than adopting a vertically integrated perspective, our model is vertically resolved, and it predicts steady-state profiles of temperature and environmental relative humidity for given profiles of large-scale vertical motion and convective mass flux.

The model consists of a simple bulk-plume representation of convection, generalizing a similar model developed by Romps (2014) for the special case of radiative-convective equilibrium (RCE). Plume models have been applied previously to examine convective onset characteristics in observations (e.g., Sahany et al., 2012; Schiro et al., 2018). Here we examine the steady-state response of convection to large-scale forcing. The bulk-plume model determines the relative humidity through a balance between convective moistening and subsidence drying in the environment (Folkins et al., 2002; Minschwaner & Dessler, 2004), and it determines the temperature by making the assumption that the cloud buoyancy is small (Bretherton & Park, 2008) as in the zero-buoyancy plume model introduced by Singh and O'Gorman (2013).

According to the bulk-plume model, the precipitation rate increases rapidly and nonlinearly with the environmental relative humidity. This relationship is similar in some respects to the observed relationship between precipitation and humidity in the tropics documented in previous studies (Bretherton et al., 2004). In the present case, however, the precipitation-humidity relationship is driven by the moistening of the environment by convective detrainment; the precipitation rate is constrained by the requirement for latent heating to balance the sum of radiative cooling and adiabatic cooling associated with the imposed large-scale forcing, and it does not depend directly on the environmental humidity. Further, the assumption of small buoyancy within the plume leads to the atmospheric lapse rate being most unstable when the relative humidity is low (Seeley & Romps, 2015), and as a result, the bulk-plume model predicts that stability increases with large-scale upward motion.

The above results are compared to a set of simulations using a CRM run to equilibrium under imposed profiles of large-scale vertical motion. These simulations were conducted as part of a proposed model intercomparison that will extend the results of the recent RCE model intercomparison project (RCEMIP; Wing et al., 2018) to include the effects of large-scale dynamics. The CRM produces relationships between precipitation, humidity, and instability similar to those predicted by the bulk-plume model, provided the simulated convection does not become organized. In order to roughly match the magnitude of the simulated humidity, the bulk-plume model must include a simple parameterization of cloud and precipitation reevaporation; a remaining challenge is to develop a more physically based method of including this effect in simple conceptual models of convection.

The rest of the paper proceeds as follows: We first derive the bulk-plume model and present the theoretical relationship between precipitation and environmental humidity (section 2). We then compare the results of the bulk-plume model to those of the CRM simulations (section 3). Finally, we present a discussion and our main conclusions (section 4).

2. Derivation of the Bulk-Plume Model

We construct a simple steady-state model for the environmental relative humidity and temperature profiles of a region of the atmosphere containing an ensemble of convective clouds under the influence of an imposed large-scale flow. Our approach follows that of Romps (2014) who derived analytical expressions for the thermodynamic structure of an atmosphere in RCE; here, we extend this work to allow for a nonzero net vertical mass flux over the domain of interest. While this generalization allows for a consideration of large-scale circulations, the steady-state assumption limits the applicability of the model to time averages longer than the time scale over which convection moistens its environment. The equilibration of our CRM simulations (see section 3.2) suggests that this time scale is of the order of 10 days. The model presented here is therefore of relevance at seasonal and intraseasonal time scales.

We represent the convective ensemble as a steady-state bulk entraining plume with an upward mass flux M_u governed by

$$\frac{\partial M_u}{\partial z} = (\varepsilon - \delta) M_u, \tag{1}$$

where ε and δ are the fractional entrainment and detrainment rates, respectively, and z is height. In this formulation, the atmosphere is divided into a cloudy region (represented by the plume) and a cloud-free environment, each with a single set of thermodynamic properties. The bulk-plume formulation therefore does not account for the heterogeneous nature of observed clouds (e.g., Paluch, 1979), but it is nevertheless commonly used as a basis for models of convective ensembles (e.g., Tiedtke, 1989).

The cloud-free environment is assumed to be subsiding, with downward mass flux M_d so that

$$M_u - M_d = M_{\text{net}}, \tag{2}$$

where M_{net} is the net vertical mass flux over the domain of interest, given by

$$M_{\text{net}} = \overline{\rho w} A \approx \overline{\rho}\ \overline{w} A. \tag{3}$$

Here ρ is the density, w is the vertical velocity, and the overbar refers to a horizontal mean over the domain of area A. Under RCE conditions, $M_{\text{net}} = 0$, and the upward mass flux within the plume is exactly balanced

by subsidence in the environment. On the other hand, for $M_{\text{net}} \neq 0$, there is a net convergence or divergence of mass into the domain. Using the steady-state continuity equation $\nabla \cdot \rho\mathbf{u} = 0$, we may relate this net divergence of mass to the vertical gradient of M_{net},

$$\oint \rho\mathbf{u} \cdot \mathbf{n} \, \mathrm{d}l = -\frac{\partial M_{\text{net}}}{\partial z}, \tag{4}$$

where $\mathbf{u}$ is the vector velocity, $\mathbf{n}$ is an outward unit normal, and the integral is taken around the boundary of the domain at a fixed level.

2.1. Relative Humidity

To derive an equation for the environmental relative humidity $\mathcal{R}$, we consider the water vapor budget of the environment, which we express as (cf. Romps, 2014)

$$-\frac{\partial}{\partial z}(M_d q_{ve}) = (\delta q_{vc}^* - \varepsilon q_{ve}) M_u + F_{ls}, \tag{5}$$

where q_{ve} is the specific humidity of the environment, q_{vc}^* is the saturation specific humidity of the plume, and F_{ls} is the flux of water vapor into the domain via the large-scale flow. Equation (5) expresses a balance between drying of the cloud environment by subsidence on the left-hand side and moistening of the environment through exchange of water vapor with the plume and large-scale fluxes on the right-hand side. Neglected in this budget is the potential source of water vapor provided by evaporation of condensate; we discuss the effects of evaporation further in section 2.4.

Following Raymond and Zeng (2005), we may use (4) to express the large-scale flux F_{ls} as

$$F_{ls} = q_x \frac{\partial M_{\text{net}}}{\partial z},$$

where q_x is the characteristic specific humidity of the air entering (for $\partial_z M_{\text{net}} > 0$) or leaving (for $\partial_z M_{\text{net}} < 0$) the domain at a given level. Substituting the above relationship into (5) and using (1) and (2), we have

$$-M_d \frac{\partial q_{ve}}{\partial z} + (q_{ve} - q_x) \frac{\partial M_{\text{net}}}{\partial z} = M_u \delta (q_{vc}^* - q_{ve}). \tag{6}$$

The second term on the left-hand side represents the effect of large-scale horizontal advection on the environmental humidity budget, and it depends on the difference between the environmental specific humidity and the humidity of air entering or leaving the domain. At levels at which the large-scale flow is divergent, it is reasonable to suppose that air leaving the domain carries with it the humidity of the cloud environment so that $q_x = q_{ve}$. For convergent flow, however, q_x represents the humidity profile of regions outside the domain of interest, and a closure assumption is required. For simplicity, we assume here that horizontal gradients of humidity are weak, and therefore, $q_x \approx q_{ve}$ under both convergent and divergent flows, allowing us to neglect the horizontal advection term and write the budget as

$$-M_d \frac{\partial q_{ve}}{\partial z} = M_u \delta (q_{vc}^* - q_{ve}). \tag{7}$$

Raymond and Zeng (2005) suggested an alternative choice in which the humidity outside the domain is taken to be equal to the humidity profile of the RCE state (i.e., the solution for $M_{\text{net}} = 0$); this approach is explored further in Appendix A.

In order to use (7) to derive an equation for the environmental relative humidity, we assume that the temperature of the plume and its environment are approximately equal (see section 2.2 below), so that we may take the saturation specific humidity of the environment to be equal to that of the plume, that is, $q_{ve}^* = q_{vc}^*$. Further approximating the environmental relative humidity as $\mathcal{R} = q_{ve}/q_{ve}^*$, we may write (7) as

$$\frac{M_d}{M_u}\left(\mathcal{R}\gamma - \frac{\partial \mathcal{R}}{\partial z}\right) = \delta(1 - \mathcal{R}), \tag{8}$$

where we have defined $\gamma = -\partial_z \ln(q_{ve}^*)$. Following Romps (2014), we assume that the relative humidity $\mathcal{R}$ varies over distances much larger than the scale height for saturation specific humidity, and we may therefore neglect vertical variations in relative humidity compared to fractional variations in specific humidity. This assumption is relatively well satisfied in our CRM simulations to be introduced in the next section,

but it may not be a good approximation in regions of the atmosphere in which different air masses exist at different levels.

The above assumption allows us to write (8) as a diagnostic for the environmental relative humidity

$$\mathcal{R} = \frac{\delta}{\delta + r\gamma}, \tag{9}$$

where $r = M_d/M_u$ is the ratio of the downward mass flux within the environment to the upward mass flux within clouds. When the atmosphere is in RCE, $r = 1$, and (9) reduces to equation (12) of Romps (2014). But if the domain is under the influence of large-scale upward motion, $M_{\text{net}} > 0$, implying that $r < 1$ and that the relative humidity is larger than its RCE value. Indeed, for very strong upward motion, the plume mass flux increasingly dominates over the environmental subsidence, $r \to 0$, and the bulk-plume model predicts that the environment approaches saturation.

2.2. Temperature

The environmental temperature profile is determined by considering an approximate equation for the moist static energy of the plume (e.g., Singh & O'Gorman, 2013)

$$\frac{\partial h_c}{\partial z} = -\varepsilon(h_c - h_e). \tag{10}$$

Here, the moist static energy is defined $h = c_p T + gz + L_v q_v$, c_p is the specific heat capacity at constant pressure, T is the temperature, g is the gravitational acceleration, L_v is the latent heat of vaporization, and the subscripts c and e refer to the plume and the environment, respectively. Following Singh and O'Gorman (2013), we assume that the mean buoyancy of clouds is small relative to the buoyancy associated with an undilute parcel ascent. Neglecting virtual temperature effects, this allows us to take the temperature of the environment T_e as being equal to the temperature of the plume T_c. This approximation is well satisfied in our CRM simulations to be presented in the next section (see Figure 5).

Since the plume is saturated above cloud base, the above assumption gives that $h_c = h_c^* = h_e^*$, and (10) may be written

$$\frac{\partial h_e^*}{\partial z} = -\varepsilon L_v q_{ve}^*(1 - \mathcal{R}), \tag{11}$$

valid above cloud base. Using the definition of moist static energy, this equation may be expressed in terms of the temperature lapse rate $\Gamma = -\partial_z T_e$ and the fractional vertical gradient of saturation specific humidity γ

$$c_p\Gamma - g + L_v q_{ve}^*\gamma = \varepsilon L_v q_{ve}^*(1 - \mathcal{R}). \tag{12}$$

To close the equation set, we construct an equation for γ by noting that

$$q_{ve}^* \approx \frac{R_d}{R_v}\frac{e_s(T_e)}{p},$$

where $e_s(T)$ is the saturation vapor pressure, p is the pressure, and R_d and R_v are the gas constants for dry air and water vapor, respectively. Taking the vertical derivative, we may use the Clausius-Clapeyron equation and hydrostatic balance to write

$$\gamma = \frac{L_v}{R_v T_e^2}\Gamma - \frac{g}{R_d T_e}, \tag{13}$$

where we have neglected virtual temperature effects.

The model for the temperature lapse rate presented here is identical to the zero-buoyancy plume model given in Singh and O'Gorman (2013). According to this model, the deviation of the tropospheric lapse rate from that of a moist adiabat increases as the relative humidity decreases. This implies that the CAPE, an integral measure of the deviation of the temperature profile from that of a moist adiabat, is larger in a drier atmosphere (Seeley & Romps, 2015). Here, the relative humidity $\mathcal{R}$ is calculated based on (9) which predicts an increase in $\mathcal{R}$ with increasing large-scale upward motion. The bulk-plume model therefore predicts that the troposphere becomes increasingly stable as the domain-mean vertical velocity increases.

2.3. Precipitation-Humidity Relationship

We now use the bulk-plume model developed above to construct a steady-state relationship between the precipitation rate averaged over the domain of interest and the environmental relative humidity. Consider the water vapor budget of the plume, which may be expressed

$$\frac{\partial(M_u q_{vc}^*)}{\partial z} = M_u(\varepsilon q_{ve} - \delta q_{vc}^*) - s_{\text{cond}},$$

where s_{cond} is the condensation rate within the plume. Using (1) and rearranging, we may write the plume condensation rate as

$$s_{\text{cond}} = M_u q_{vc}^* \left[\gamma - \varepsilon(1 - \mathcal{R})\right]. \tag{14}$$

Since the plume model, as described in the previous subsections, does not include any evaporation of condensed water within the environment, s_{cond} represents the net condensation rate at a given level. We consider the effects of precipitation reevaporation in more detail in the next section, but for the moment, we may take the surface precipitation rate as the vertical integral of s_{cond}.

In order to derive an analytic formula relating the precipitation rate to the environmental relative humidity, we make a number of simplifying assumptions. Note that these assumptions are only applied for the purposes of deriving a simple formula for relating precipitation to relative humidity in steady state; they are not needed in our application of the vertically resolved bulk-plume model to CRM simulations in the next section. We first assume that $|\partial_z \ln M_u| << \varepsilon$ so that $\varepsilon \approx \delta$ within the troposphere. This assumption is valid provided the tropospheric mass flux varies over vertical scales that are large compared to $1/\varepsilon$. This is roughly the case in our simulations described in the next section, where $|\partial_z \ln M_u|$ averaged over the lower troposphere is $\lesssim 0.2\ \text{km}^{-1}$, while we set $\varepsilon = 0.7\ \text{km}^{-1}$. But it may not be an appropriate assumption in cases where the mass flux has strong vertical structure. Our second assumption is that the downward mass flux in the environment remains fixed at its RCE value irrespective of the upward mass flux in the plume. That is, we set $M_d = M_{\text{RCE}}$, where M_{RCE} is the cloud mass flux under RCE conditions, for which $r = 1$. This approximation is valid if it may be assumed that the downward mass flux is set by a balance between radiative cooling and subsidence in the environment and that the radiative cooling rate itself is fixed. This approximation is not valid if evaporation within the environment is considered, as the associated latent cooling affects the environmental heat budget (see section 2.4 and Appendix B).

The above assumptions imply that $M_u = M_{\text{RCE}}/r$ and allow us to write the plume condensation rate as

$$s_{\text{cond}} = M_{\text{RCE}} q_{vc}^* \gamma \left(\frac{1}{r}\right)\left[1 - \frac{\delta}{\gamma}(1 - \mathcal{R})\right].$$

Using the diagnostic equation for the environmental relative humidity (9), we may express r and δ/γ in terms of $\mathcal{R}$, the relative humidity, and $\mathcal{R}_{\text{RCE}}$, the relative humidity under RCE conditions (for which $r = 1$)

$$r = \frac{\delta}{\gamma}\frac{1 - \mathcal{R}}{\mathcal{R}},$$

$$\frac{\delta}{\gamma} = \frac{\mathcal{R}_{\text{RCE}}}{1 - \mathcal{R}_{\text{RCE}}}.$$

Combining the previous three equations and taking the vertical integral, we may construct an equation for the precipitation rate P

$$P = \langle M_{\text{RCE}} q_{vc}^* \gamma \rangle \left(\frac{\mathcal{R}}{\mathcal{R}_{\text{RCE}}}\right)\left[\frac{1 - 2\mathcal{R}_{\text{RCE}} + \mathcal{R}\mathcal{R}_{\text{RCE}}}{(1 - \mathcal{R})}\right],$$

where we have defined the angle brackets as a vertical integral from cloud base to the top of the convecting layer, and we have neglected vertical variations in relative humidity. The above equation may be cast in a simpler form by nondimensionalizing the precipitation rate by its RCE value P_{RCE}

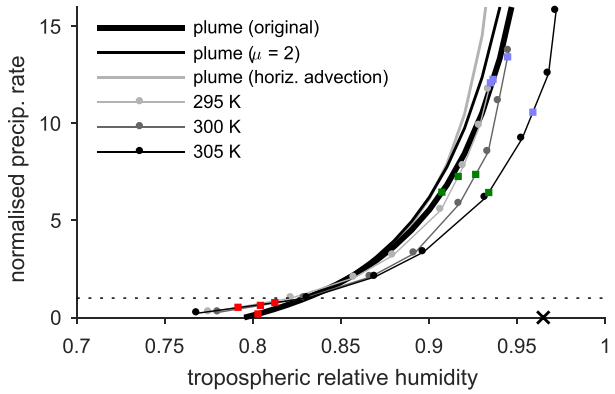

Figure 1. Relationship between domain-averaged precipitation rate (normalized by its RCE value) and tropospheric environmental relative humidity according to the bulk-plume model (solid lines) and in CRM simulations with varying large-scale forcing strength w_0 and for different SSTs given in the legend (lines with symbols). Thick black line shows bulk-plume model prediction without evaporation or horizontal advection (15), thin black line shows bulk-plume model prediction including evaporation (B2; $\mu = 2$), and gray line shows bulk-plume model prediction including horizontal advection (A1; $B = 1.28$). In all cases $\mathrm{R_{RCE}}$ is set equal to 0.83. Cross on the x-axis shows $\mathrm{R_{max}}$ according to (A.2). The simulated precipitation curves are normalized by the RCE precipitation rates of 2.2, 2.7 and 3.4 mm day^{-1} in the 295-K, 300-K and 305-K simulations, respectively. Squares show the location of the point at which r = 1.2 (red), 0.5 (green) and 0.33 (blue) (estimated by linear interpolation in relative humidity). Simulated quantities are plotted as time means over last 50 days, and the simulated value of r is calculated as a mass-weighted mean from z_b to z_t.

$$\frac{P}{P_{\mathrm{RCE}}} = \frac{\mathcal{R}}{\mathcal{R}_{\mathrm{RCE}}}\left[1 + \frac{\mathcal{R} - \mathcal{R}_{\mathrm{RCE}}}{(1-\mathcal{R})(1-\mathcal{R}_{\mathrm{RCE}})}\right]. \tag{15}$$

This relationship is plotted in Figure 1 for the case $\mathcal{R}_{\mathrm{RCE}} = 0.83$. The bulk-plume model predicts that the precipitation rate increases rapidly with the environmental relative humidity, with the precipitation rate approaching infinity as the troposphere approaches saturation. Physically, the sharp increase of precipitation with relative humidity may be understood to be a result of the separate dependencies of the steady-state precipitation rate and the steady-state relative humidity on the large-scale vertical velocity. An increase in the large-scale vertical velocity is associated with an increase in cloud mass flux M_u, which, by (14), is associated with an increase in the condensation rate, implying stronger precipitation. At the same time, an increase in large-scale vertical velocity implies a decrease in r, a weakening of the subsidence drying relative to the detrainment moistening in the environment and a corresponding increase in the relative humidity via (9). Since $\mathcal{R}$ reaches saturation as $r = M_d/M_u \to 0$, the mass flux (and the precipitation rate) increase without bound as the atmosphere approaches saturation.

For large-scale descent ($M_{\mathrm{net}} < 0$), both the relative humidity and precipitation rate decrease below their RCE value, until the precipitation rate becomes zero at a relative humidity given by

$$\mathcal{R}_{\mathrm{min}} = 2 - \frac{1}{\mathcal{R}_{\mathrm{RCE}}},$$

if $\mathcal{R}_{\mathrm{min}} > 0$ or at $\mathcal{R} = 0$ otherwise. The bulk-plume model therefore only produces physical solutions for $\mathcal{R} > \mathcal{R}_{\mathrm{min}}$.

More generally, the bulk-plume model predicts that steady-state convection can only be maintained when the condensation rate within the plume $s_{\mathrm{cond}} > 0$. Using (14), this condition may be expressed as

$$\gamma > (\varepsilon - \delta) + \delta\left(\frac{r-1}{r}\right). \tag{16}$$

The above equation generalizes a similar constraint derived by Romps (2014) for the case of RCE (their equation 15). Assuming $\varepsilon \approx \delta$, (16) may be violated for sufficiently strong large-scale descent (i.e., r sufficiently large). Under these conditions, convection and its associated moistening of the troposphere is suppressed, the bulk-plume model is no longer valid, and the steady-state environmental humidity budget can only be solved if the environmental specific humidity becomes a constant equal to its value at the tropopause.

The relationship (15) was derived for a steady-state atmosphere and by making a number of further simplifying assumptions that may not be applicable to Earth's tropics. Nevertheless, this simple equation predicts a strong relationship between precipitation and environmental humidity that is in some respects similar to the observed relationship between precipitation and humidity over the tropical oceans (Bretherton et al., 2004). The steady-state framework discussed here may therefore be a useful limit to consider in understanding the factors that control the precipitation-humidity relationship in climate models and in the observed atmosphere on long time scales.

2.4. Evaporation in the Environment

In our derivation of the bulk-plume model above, we assumed that the only source of water vapor in the environment is the detrainment of water vapor from clouds. But clouds also detrain condensed water, and the evaporation of this condensed water provides an additional source of water vapor in the environment. This evaporative source may be included in the environmental water vapor budget as an extra term on the right-hand side of (7)

$$-M_d \frac{\partial q_{ve}}{\partial z} = M_u \delta (q^*_{vc} - q_{ve}) + s_{\text{evap}}. \tag{17}$$

In general, the magnitude of the source s_{evap} depends on the detailed microphysical properties of clouds and precipitation, and its representation within a bulk-plume model must necessarily be a crude approximation. For example, Romps (2014) took s_{evap} to be a fixed fraction of the gross condensation rate at each level. A limitation of this approach is that, for strong large-scale ascent (for which $r < 1$), it predicts relative humidities greater than unity. This is because the evaporative source of water vapor does not approach zero as the environment approaches saturation.

Here, we take a different but equally crude approach, and we assume that

$$s_{\text{evap}} = \mu \delta M_u q^*_{vc} (1 - \mathcal{R}), \tag{18}$$

where μ is a nondimensional parameter representing the importance of the evaporative source of water vapor. The parameterization (18) may be considered to be the result of two assumptions: (1) That the detrainment flux of condensed water into the environment is proportional to the detrainment flux of water vapor into the environment at each level, and (2) that the fraction of this condensed water flux that evaporates within the environment at the level at which it is detrained is proportional to $(1 - \mathcal{R})$, while the rest of the detrained condensate precipitates to the surface. Adopting this parameterization and modifying the arguments of section 2.1 to allow for the evaporative source, it may be shown that the environmental relative humidity is given by

$$\mathcal{R} = \frac{\delta_T}{\delta_T + r\gamma}, \tag{19}$$

where $\delta_T = \delta(1 + \mu)$ represents the "total" detrainment rate, including detrainment of condensates that evaporate in the environment. The original expression (9) for $\mathcal{R}$ may then be considered to be the special case in which $\mu = 0$.

The assumptions leading to (19) neglect the details of vertical transport of condensed water within the plume and its environment. However, the resultant parameterization has the advantage that the evaporative source approaches zero as the environment approaches saturation, ensuring that the relative humidity remains less than unity, even under strong large-scale upward motion (provided r remains positive). A disadvantage of our parameterization is that the evaporation rate s_{evap} does not depend explicitly on the condensation rate within the plume s_{cond}. In particular, when evaporation is included, the net condensation rate at a given level s_{net} is equal to the plume condensation rate (14) minus the evaporation in the environment (18)

$$s_{\text{net}} = M_u q^*_{vc} \left[\gamma - (\varepsilon + \mu\delta)(1 - \mathcal{R}) \right]. \tag{20}$$

Under large-scale descent, the evaporation rate increasingly dominates over the plume condensation rate, and for sufficiently strong large-scale descent, the plume condensation rate and the environmental evaporation rate are equal, and the implied precipitation efficiency is reduced to zero. Indeed, convection can be maintained only when the net condensation rate is positive, requiring that

$$\gamma > (\varepsilon - \delta) + \delta_T \left(\frac{r - 1}{r} \right). \tag{21}$$

Comparing this equation to (16), it may be seen that the relative humidity below which convection cannot be maintained in the steady-state bulk-plume model is sensitive to our parameterization of environmental evaporation. We therefore do not expect the bulk-plume model to be accurate in the case of large-scale descending motion; we discuss this further when we compare the bulk-plume model to CRM simulations in the next section.

The inclusion of the evaporative source s_{evap} does not alter the equation for the temperature lapse rate (12), except implicitly by the altered expression for the relative humidity. The derivation of the predicted relationship between precipitation and environmental relative humidity (15) may also proceed similarly, with two caveats. First, as mentioned above, the value of $\mathcal{R}_{\text{min}}$ at which convection can no longer be maintained is strongly sensitive to the evaporation parameterization. Second, the assumption that the downward mass flux in the environment M_d remains fixes at its RCE value is no longer valid; we now must consider evaporative cooling in the environmental heat budget. As shown in Appendix B, one can approximately account for the effect of this environmental cooling in determining the downward mass flux, but this turns out to have a relatively weak effect on the overall precipitation-humidity relationship (Figure 1).

2.5. Summary

We have presented a steady-state bulk-plume model for the temperature and relative humidity structure of the atmosphere under the influence of large-scale vertical motion. The inputs to this model are the large-scale vertical velocity $\overline{w}$, the convective mass flux M_u, the entrainment rate ϵ, and the evaporation parameter μ. Using (1)–(3), (12), (13), (19), and hydrostatic balance, the profiles of temperature and environmental relative humidity from cloud base to the top of the convecting layer may then be derived (see Appendix C for details). Under some additional assumptions, the bulk-plume model may be simplified to give a one-parameter family of curves (15) for the steady-state precipitation rate, relative to its RCE value, as a function of the tropospheric relative humidity. In the next section, we will compare the results from this bulk-plume model to simulations using a CRM with imposed large-scale vertical motion.

3. Comparison to CRM Simulations

3.1. Simulation Design

We conduct simulations of an ensemble of convective clouds under the influence of an imposed profile of large-scale vertical motion using the System for Atmospheric Modeling Version 6.11.1 (SAM; Khairoutdinov & Randall, 2003). SAM is a three-dimensional, anelastic CRM that solves prognostic equations for momentum, liquid/ice water static energy, and precipitating and nonprecipitating water concentrations. The model is formulated so that the liquid/ice water static energy is conserved for adiabatic processes, including condensation and freezing. SAM includes a single-moment microphysics scheme in which the hydrometeor partitioning is determined as a simple function of temperature, and it includes a Smagorinsky turbulence scheme to account for subgrid-scale motions. Full details may be found in Khairoutdinov and Randall (2003).

Simulations are conducted on a doubly periodic 96×96 km domain with a horizontal grid spacing of 1 km and with 74 unevenly spaced vertical levels. The vertical grid spacing stretches from 75 m at the surface to 500 m at 3 km, above which it is constant to the model top of 33 km. Newtonian damping is applied to the winds in the top 30% of the domain to eliminate gravity-wave reflection. The lower-boundary condition is assumed to be a sea surface with a fixed temperature; fluxes of energy, water vapor, and momentum between the surface and the atmosphere are parameterized using bulk aerodynamic formulae with a minimum wind speed of 1 m s^{-1} and with exchange coefficients calculated using Monin-Obukov similarity theory. Radiative heating and cooling is calculated via the RRTMG longwave and shortwave radiation scheme (Clough et al., 2005), and simulations are conducted without a diurnal cycle, with the top-of-atmosphere solar insolation held fixed at 551.58 W m^{-2} incident at a zenith angle of 42.05°.

Our simulations follow a proposed intercomparison of limited-domain models to be described in a forthcoming publication. This intercomparison aims to extend the recent RCEMIP protocol for CRMs run in an RCE configuration (Wing et al., 2018), to explore the response of CRMs, as well as single-column models, to steady large-scale forcing. Specifically, we impose a domain-mean vertical velocity with first baroclinic mode structure given by

$$\overline{w} = w_0 \sin\left(\frac{\pi z}{H}\right), \tag{22}$$

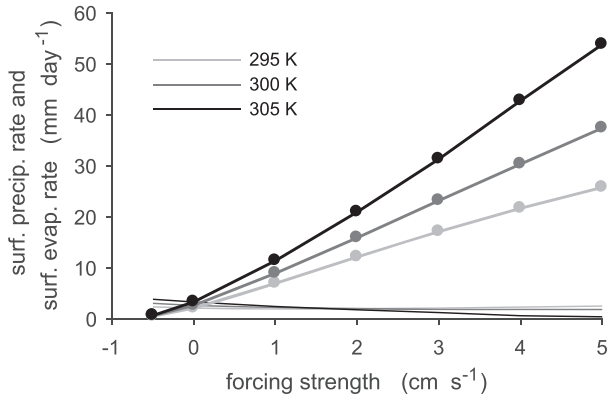

Figure 2. Domain- and time-mean surface precipitation rate (thick lines with symbols) and surface evaporation rate (thin lines) for the last 50 days of CRM simulations as a function of the forcing strength w_0 and for different SSTs as given in the legend.

as a time-invariant forcing to the simulations. Here, the forcing is applied at heights $z < H$, and its strength is given by w_0. The forcing is implemented as an additional tendency to the temperature T and specific humidity q_v so that

$$\left.\frac{\partial T}{\partial t}\right|_{\text{forcing}} = -\overline{w}\left(\frac{\partial \overline{T}}{\partial z} + \frac{g}{c_p}\right), \tag{23a}$$

$$\left.\frac{\partial q_v}{\partial t}\right|_{\text{forcing}} = -\overline{w}\frac{\partial \overline{q_v}}{\partial z}. \tag{23b}$$

The above implementation neglects vertical advection of condensed water and momentum by the imposed large-scale vertical velocity, and it applies the same advective tendency to all grid points at a given level in the domain, thereby neglecting horizontal variations in temperature and humidity when evaluating the forcing. The effects of these approximations on the resultant convection are explored further in section 3.4. Consistent with the bulk-plume model derived in section 2, (23) also neglects large-scale horizontal advection of temperature and humidity.

As in the original RCEMIP protocol, we conduct simulations at three different SSTs (295, 300, and 305 K). At each SST, we conduct a series of simulations with w_0 ranging from −0.5 to 5 cm s^{-1}, including the RCE case in which $w_0 = 0$ cm s^{-1}. The RCE simulations are initialized with the analytic temperature and moisture profiles given in Wing et al. (2018), and all other simulations are initialized using time- and domain-mean profiles from the equilibrated RCE simulation at the same SST. The value of H is set to 11, 12.5, and 14 km in the simulations with SSTs of 295, 300, and 305 K, respectively. This is based roughly on the level to which the convective clouds reach in the RCE simulations.

Each simulation is run for 100 days, with the last 50 days used to construct time-averaged statistics. Statistics presented are therefore a representation of the steady-state response to imposed forcing, although even after 50 days, there is some drift in domain-mean quantities in the warmest and most strongly forced cases (not shown).

In addition to the simulations using SAM described above, we have also conducted a similar suite of simulations with varying large-scale forcing using the Bryan Cloud Model (CM1; Bryan & Fritsch, 2002) to test the sensitivity of our results to model formulation. The overall response to large-scale forcing is similar across both models, and so we focus on the SAM simulations in the quantitative results shown in the next subsections, but we note in the text specific aspects of the results that differ depending on the CRM used.

3.2. Approach to Equilibrium

Before we examine the steady-state results, we briefly consider the time scale over which the simulations approach equilibrium. This time scale provides a rough guide to the minimum temporal-averaging period for which the steady-state bulk-plume model may be applicable to the tropical atmosphere. We estimate the

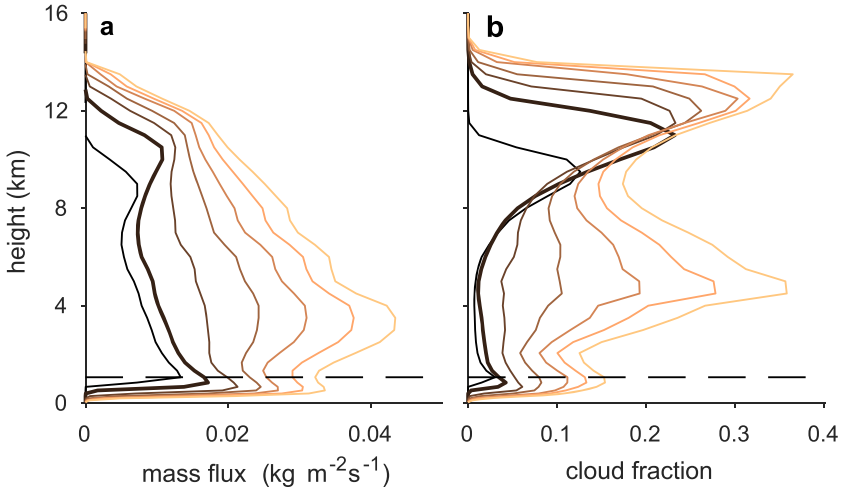

Figure 3. Time- and domain-mean profiles of (a) cloud mass flux per unit area and (b) cloud area fraction over the last 50 days of CRM simulations with SST of 300 K and w_0 values of −0.5 (black), 0, 1, 2, 3, 4, and 5 (orange) cm s^{-1} (thick line gives RCE case). Horizontal dashed line shows the level $z = 1,062$ m at which the bulk-plume model is initialized.

equilibration time scale τ by fitting an exponential curve to the time series of the domain-averaged CWV with its mean over the last 50 days subtracted. This fit is performed based on output from Days 2 to 20 of each simulation. For the 300 K simulations, τ increases from 6 days in the $w_0 = -0.5$ cm s^{-1} simulations to 20 days in the case with the strongest large-scale upward motion. These results suggest that the steady-state picture examined in this paper may be of relevance for the climatology, as well as seasonal and intraseasonal variability in the tropics.

3.3. Steady-State Results

The simulated steady-state response of the domain-mean surface precipitation and surface evaporation rates to the imposed large-scale forcing is shown in Figure 2. The precipitation rate increases roughly linearly with the forcing strength, and, for all SSTs, it is at least 10 times larger in the simulation with the strongest large-scale forcing ($w_0 = 5$ cm s^{-1}) compared to the RCE case. In contrast, the surface evaporation rate remains similar to, or lower than, its RCE value as the forcing strength is varied. This imbalance between the mean precipitation and evaporation rates for $w_0 > 0$ is associated with convergence of moisture into the column by the imposed profile of large-scale upward motion. Conversely, in the $w_0 = -0.5$ cm s^{-1} case, surface evaporation exceeds surface precipitation due to divergence of moisture from the column.

The large increase in precipitation rate with forcing strength is associated with a similarly large increase in both the cloud mass flux and cloud area fraction as w_0 is increased (Figure 3). For example, in the 300 K simulations, the mean cloud fraction at 2 km increases from 0.02 to 0.13 as w_0 is increased from 0 to 5 cm s^{-1}, while the mean in-cloud vertical velocity actually decreases (see also section 4). Here, a gridbox is identified as cloudy if it has a cloud water (liquid or solid) concentration greater than a threshold q_{thresh} given by

$$q_{\text{thresh}} = \min\left[10^{-5},\ \frac{q_v^{*l}(\overline{T},\overline{p})}{100}\right],$$

where $q_v^{*l}(\overline{T},\overline{p})$ is the saturation specific humidity with respect to liquid evaluated at the domain-mean temperature and pressure at each level.

Snapshots of the cloud field reveal that, as the large-scale upward motion increases, both the size and number of cloudy regions increase (Figure 4, contours). However, even at strong large-scale forcing, the convection remains relatively disorganized and evenly spread out over the domain. The simulations show little evidence of convective self-aggregation, a state characterized by a small region of active convection surrounded by a relatively dry region with no precipitation (e.g., Bretherton et al., 2005).

The snapshots also reveal that the relative humidity outside of clouds increases with increasing large-scale upward motion (Figure 4, shading), consistent with the prediction of the bulk-plume model. Indeed, for the 300 K case, the environmental relative humidity increases monotonically with w_0 at almost all heights,

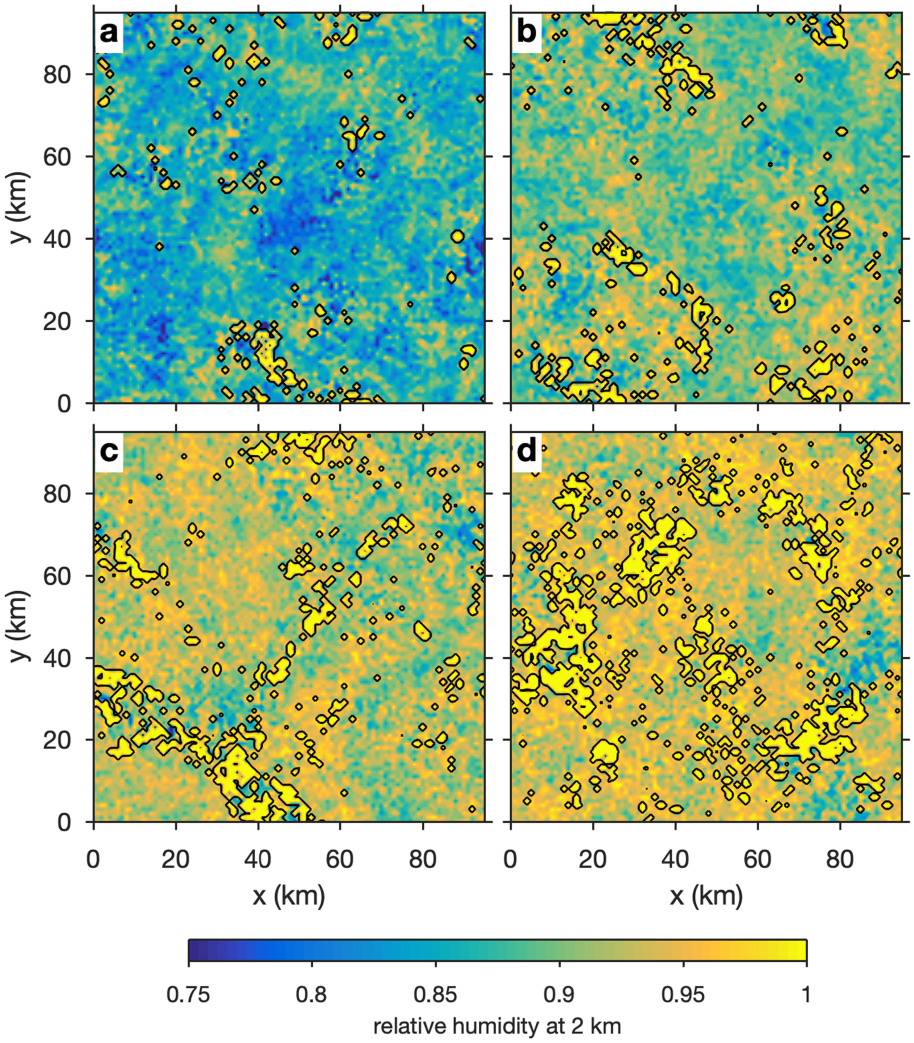

Figure 4. Snapshots of relative humidity (q_v/q_v^*) at 2,055 m (colors) at Day 75 of CRM simulations with SST = 300 K and w_0 equal to (a) 0, (b) 1, (c) 3, and (d) 5 cm s^{-1}. Cloudy regions are demarcated by the black contour.

except near to the tropopause (Figure 5a). To be consistent with the bulk-plume model, we define the environmental relative humidity in the simulations as a ratio of specific humidities

$$\mathcal{R} = \frac{q_{ve}}{q_v^*(\overline{T}, \overline{p})},$$

where the overbar refers to a time- and domain-mean and the subscript e refers to a time- and domain-mean over cloud-free gridboxes. The saturation specific humidity is calculated including ice and following SAM's saturation adjustment scheme with a mixed-phase range between 253.16 and 273.16 K.

We compare the simulated environmental relative humidity profiles to those predicted by the bulk-plume model quantitatively in Figures 5a and 5b. The bulk-plume model is solved by taking as inputs the large-scale vertical velocity profile (22) and the mass flux profile, given by the mean upward mass flux in cloudy regions in the corresponding simulation (Figure 3a). The entrainment and evaporation parameters are then set to be constants given by $\varepsilon = 0.7$ km^{-1} and $\mu = 2$, respectively, to give a good overall fit to the simulations. Given these inputs, the bulk-plume model is integrated from a nominal cloud base at $z_b = 1,062$ m to the level z_t at which the simulated cloudy mass flux decreases to zero; full details of the solution method are provided in Appendix C.

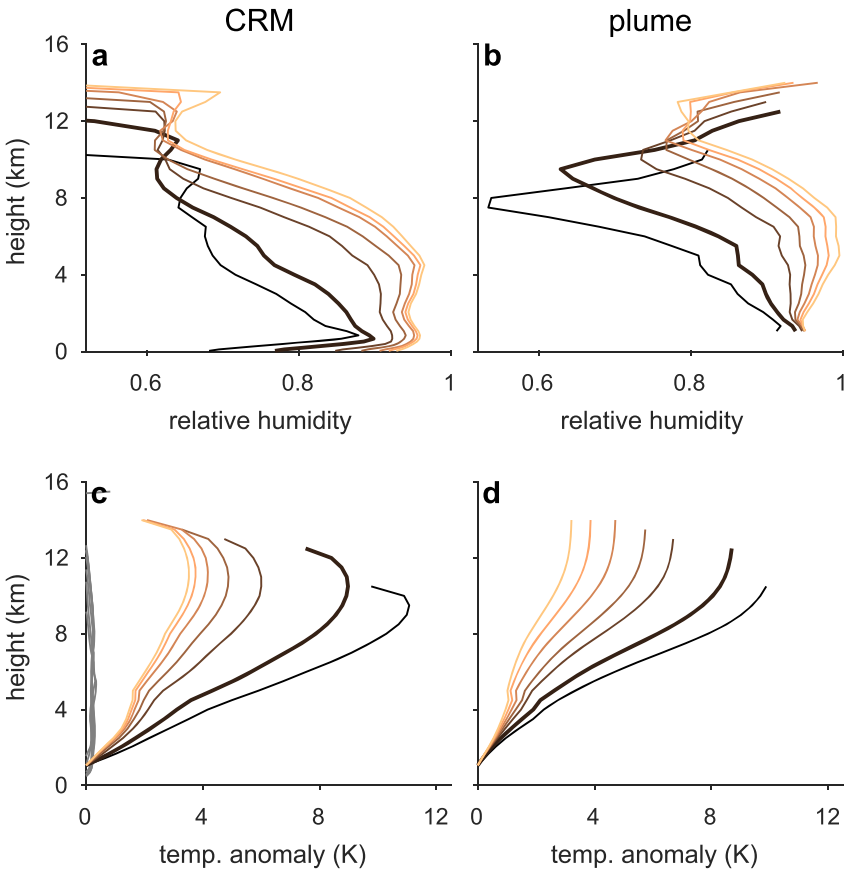

Figure 5. Profiles of (a,b) environmental relative humidity and (c,d) temperature excess of an undiluted plume δT for SST of 300 K and w_0 values of −0.5 (black), 0, 1, 2, 3, 4, and 5 (orange) cm s^{-1} (thick line gives RCE case) in CRM simulations (left) and according to the bulk-plume model (right). Simulated profiles are taken as the mean over the last 50 days of each simulation. Gray curves in (c) show simulated temperature excess within cloud cores (cloudy gridpoints with $w > 1$ m s^{-1}) for each CRM simulation.

For the 300-K case, the bulk-plume model is able to reproduce the basic features of the simulated relative humidity profiles and their variation with the large-scale forcing, including the overall shape of the relative humidity profile in RCE (as also found in Romps, 2014) and the rough magnitude of the increase in midtropospheric relative humidity with increasing forcing strength w_0. On the other hand, compared to the simulations, the bulk-plume model overestimates the sensitivity of relative humidity to w_0 in the upper troposphere and underestimates it near cloud base. Furthermore, while the simulated midtropospheric relative humidity becomes insensitive to the forcing strength at high w_0 values, the bulk-plume model predicts that the relative humidity continues to increase as the forcing is increased to $w_0 = 5$ cm s^{-1}. Finally, at the top of the convecting layer, the bulk-plume model predicts that the environmental relative humidity approaches saturation, while in the simulations, $\mathcal{R}$ remains below 0.7 even for strong forcing. It should be noted, however, that the upper tropospheric relative humidity in our RCE simulation is considerably lower than found using CM1 (see also Romps, 2014) and in simulations with SAM at higher vertical resolution (not shown). The reasons for this sensitivity of the upper-tropospheric humidity to model and resolution is the subject of current study. Despite the differences mentioned above, the fidelity of the bulk-plume model in reproducing the results of the CRM simulations is impressive given its simplicity.

The bulk-plume model also provides a prediction for the mean temperature profile of the atmosphere, and this prediction is compared to the simulated temperature profiles for the 300 K case in Figures 5c and 5d. To focus on the deviation of the temperature profile from that of a moist adiabat, we plot the temperature excess

$$\delta T = T_u - \overline{T},$$

where T_u is the temperature of a moist adiabat, approximated as the temperature of an undiluted plume initialized at saturation at the level z_b. The temperature of this undiluted plume is calculated identically to the bulk-plume model but with the entrainment rate set to zero.

For both the simulations and the bulk-plume model, $\delta T > 0$ throughout the troposphere, implying that the mean temperature is lower than that of an undiluted plume and that the CAPE of the mean state is nonzero. The temperature excess δT is much larger than the temperature difference between updraft cores (defined as cloudy gridpoints in which $w > 1$ m s^{-1}) and the domain mean, justifying our assumption of small cloud buoyancy in the bulk-plume model (gray lines on Figure 5c; similar results are obtained if virtual temperatures are used).

The simulated temperature excess decreases as the forcing strength w_0 is increased, and this behavior is well reproduced by the bulk-plume model. Indeed, both the simulations and the bulk-plume model predict that the atmospheric lapse rate is most unstable under large-scale subsidence, when the tropospheric relative humidity is low.

A similar relationship between atmospheric instability and the dryness of the troposphere has been found in idealized simulations of RCE (Seeley & Romps, 2015; Singh & O'Gorman, 2013) and in observations of precipitating regions of the tropics (Singh et al., 2017). Such results may be understood in the context of the bulk-plume model by examining its governing equation for moist static energy. According to (11), the deviation of the atmosphere from moist neutrality is dependent on the environmental saturation deficit; this saturation deficit increases with temperature and with decreasing relative humidity (Singh & O'Gorman, 2013). Since the bulk-plume model predicts that the relative humidity increases with w_0, it also predicts that the atmospheric lapse rate becomes more stable as the forcing strength is increased.

While we have focused here on the 300 K case, the results for other SSTs are similar; in all cases, the simulated relative humidity increases with the forcing strength w_0 at almost all heights in the troposphere, while the temperature excess δT decreases. Consistent with previous work (Seeley & Romps, 2015; Singh & O'Gorman, 2013), the simulated temperature excess becomes larger as the atmosphere warms and the saturation deficit between clouds and their environment increases. These features are broadly captured by the bulk-plume model, although it should be noted that for both the 295 and 305 K cases, the bulk-plume model predicts relative humidities greater than one under the strongest large-scale forcing. Such relative humidity values are unphysical and lead to the plume importing moisture from its environment, but they are predicted by the bulk-plume model if the diagnosed cloud mass flux within the simulation is smaller than $\overline{\rho w}$, and as a result, the environment is diagnosed as ascending rather than descending.

We now evaluate the theoretical relationship between relative humidity and precipitation (15) derived based on the bulk-plume model. Plotted on Figure 1 along with (15) is the simulated time- and domain-mean precipitation rate as a function of the tropospheric relative humidity, which we define

$$\mathcal{R}_{\text{trop}} = \frac{\langle q_{ve} \rangle}{\langle q_v^*(\overline{T}, \overline{p}) \rangle},$$

where the angle brackets represent a mass-weighted integral from the cloud base z_b to the height z_t at which the cloud mass flux is reduced to zero. Also given on Figure 1 are estimates of values of $r = 1.2, 0.5$, and 0.333 along each curve.

For large-scale upward motion, the simulated relationship between precipitation and tropospheric relative humidity is broadly similar to the theoretical prediction (15). In both cases, the precipitation rate increases rapidly with relative humidity, with the rate of increase being largest at high relative humidity. Note, however, that while the tropospheric relative humidity $\mathcal{R}_{\text{trop}}$ increases monotonically with the precipitation rate [and hence the forcing strength] at all SSTs, the relationship between CWV and w_0 is nonmonotonic for SST = 295 K [not shown]. This nonmonotonicity of precipitation with CWV is also present in simulations using CM1, and it is a result of a decrease in the column-mean temperature with increasing w_0 leading to a reduction in CWV despite a concurrent increase in $\mathcal{R}_{\text{trop}}$.

Some details of the simulated precipitation-relative humidity relationship are not captured by (15). For example, while (15) contains no explicit dependence on surface temperature, except through its dependence on $\mathcal{R}_{\text{RCE}}$ which varies by less than 1% across the simulations, the rate of increase of precipitation with relative humidity appears to decrease systematically with surface temperature in the SAM simulations. This behav-

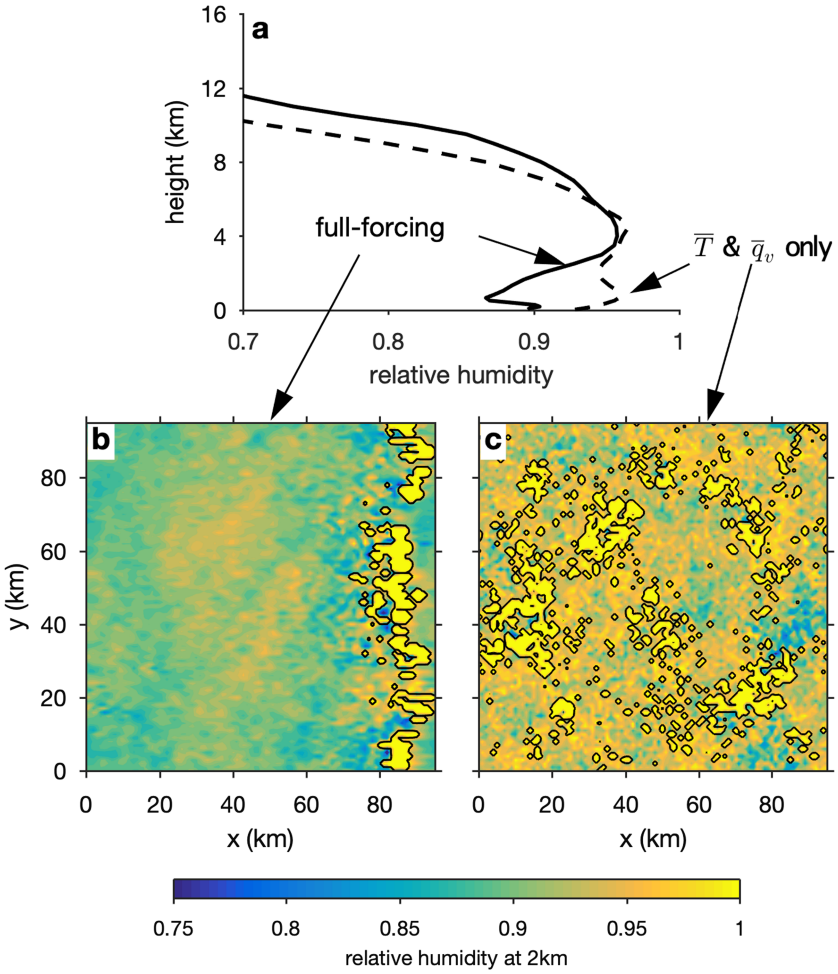

Figure 6. (a) Time-mean environmental relative humidity profiles for SST = 300 K and $w_0 = 5$ cm s^{-1} in "standard" simulation, in which the forcing is applied to the domain-mean temperature and humidity following (23) (dashed), and in "full-forcing" simulation, in which the forcing is also applied to condensed water, momentum, and horizontal variations in temperature and humidity (solid). (b,c) Corresponding snapshots of the relative humidity (colors) and boundary of cloudy regions (black contour) at 2,055 m and at Day 75 for the (b) full-forcing and (c) standard cases.

ior appears to be somewhat model dependent [simulations with CM1 do not exhibit the same temperature dependence], and also contrasts with observational studies, which find that deep convective onset occurs in conditions farther from saturation when the temperature is higher (Kuo et al., 2018; Sahany et al., 2012). Thus, while the theoretical relationship (15) provides a good first-order explanation for the steady-state relationship between precipitation and humidity in our simulations with large-scale ascent, it does not account for the precise rate at which the precipitation rate increases with $\mathcal{R}_{\text{trop}}$ or its variation in different climates.

For the case of large-scale descent, the simulated precipitation rate and relative humidity both decrease from their RCE values, as expected from (15). If the magnitude of this descent is increased even slightly so that $w_0 = -0.6$ cm s^{-1}, deep convection in the domain shuts off, and a steady state cannot be maintained; the precipitation rate gradually reduces to ~0.1 mm day^{-1} over the course of the simulation (not shown). These results are qualitatively consistent with (15), which shows the precipitation rate rapidly decreasing to zero as the relative humidity decreases to $\mathcal{R}_{\text{min}} = 0.80$ under large-scale descent. However, the bulk-plume model is not quantitatively accurate; it is clear from Figure 1 that steady-state convection can be maintained in the simulations at tropospheric relative humidities substantially below $\mathcal{R}_{\text{min}}$. As we show below, the predicted minimum relative humidity for which steady-state convection is possible is highly sensitive to the parameterization of evaporation used in the bulk-plume model.

As discussed in section 2.4, the evaporation parameterization used in the bulk-plume model implies that the precipitation efficiency ($\langle s_{net} \rangle / \langle s_{cond} \rangle$) decreases to zero as $\mathcal{R} \to \mathcal{R}_{min}$. But this is not the only possible choice. An alternative parameterization could instead ensure that the precipitation efficiency remains positive, by, for example, allowing μ to decrease with increasing large-scale descent. For this alternative parameterization, the net condensation rate remains positive (and steady-state convection remains possible) as long as $s_{cond} > 0$. Assuming $\epsilon \approx \delta$ and taking $\mathcal{R}_{RCE} = 0.83$ as before, (14) may be used to show that the condition $s_{cond} > 0$ is satisfied down to a relative humidity of approximately 0.39. In this calculation, we assume $\mu = 2$ in the RCE state and therefore $\mathcal{R}_{RCE} = \frac{3\delta}{\gamma+3\delta}$. It may then be shown that $s_{cond} = 0$ when $\mathcal{R} = 1 - \frac{\gamma}{\delta} = \frac{4\mathcal{R}_{RCE}-3}{\mathcal{R}_{RCE}}$=0.39. This is substantially lower than the lowest steady-state relative humidity we were able to simulate with the CRM, and it is close to a factor of 2 smaller than $\mathcal{R}_{min}$ as defined above. These results highlight the sensitivity of the bulk-plume model to the evaporation parameterization in the limit of strong large-scale descent. Further work is required to construct a parameterization of evaporation in the environment that is both simple and physically realistic under all circumstances.

3.4. Effect of Convective Organization

As pointed out in the previous subsection, the convection in our standard set of simulations with SAM remains relatively disorganized even when the forcing is strong and the domain-mean precipitation increases to rates in excess of 40 mm day^{-1} (see Figure 4). However, further exploration has revealed that this result is not robust to the CRM used (SAM vs. CM1) or even to the method of applying the large-scale forcing. In particular, we have conducted an alternate set of simulations identical to the 300 K simulations described above except that (1) the large-scale vertical velocity is allowed to advect momentum and condensed water in addition to temperature and water vapor and (2) the forcing is allowed to act on the full fields rather than only their domain means as is the case in (23). In these "full-forcing" simulations, convection organizes into structures resembling squall lines at values of $w_0 \geq 4$ cm s^{-1} (Figures 6b and 6c), and the domain-mean winds strengthen to be ~10 m s^{-1} in the lower troposphere. While understanding the mechanisms producing such squall lines requires further work, we speculate that by allowing the large-scale vertical velocity to advect condensed water and anomalies in water vapor, the moistening effect of the forcing is amplified in regions that are already moist, favoring convective aggregation.

Importantly for the present study, the presence of organization appears to have an effect on the domain-mean thermodynamic profiles. For the most strongly forced case, the environmental relative humidity in the lower troposphere is ~5% lower in the full-forcing (organized) simulation than in the corresponding standard (disorganized) case (Figure 6a). Since the squall-line-like features only appear at high values of w_0, this results in nonmonotonic behavior of the lower-tropospheric relative humidity with w_0 in the full-forcing simulations. In the context of the bulk-plume model, these results may be interpreted as a change in the entrainment rate due to changes in the morphology of clouds. The differences in domain-mean quantities as a result of changes to details of the forcing implementation highlights the potential role of small-scale convective processes in influencing the large-scale thermodynamic state of the atmosphere, even when the large-scale flow is fixed.

3.5. Cloud-Scale Vertical Velocity

According to both the bulk-plume model and CRM simulations, the tropospheric lapse rate becomes more stable as the large-scale forcing is increased. This suggests, somewhat paradoxically, that the potential for strong cloud-scale updrafts is highest under large-scale descent. Indeed, in the CRM simulations, the mean vertical velocity within cloud cores decreases monotonically with forcing strength in the lower to middle troposphere, and it peaks in the simulation forced by large-scale descent (Figure 7a). (Here, cloud cores are defined as cloudy gridpoints in which the vertical velocity is greater than 1 m s^{-1}.) Since the cloud mass flux increases roughly linearly with w_0 (Figure 3), this implies that variations in simulated cloud mass flux are driven primarily by changes in cloud area fraction rather than changes in cloud updraft velocity. A similar conclusion has been drawn from observed estimates of convective mass flux and its variability derived from radar observations within the tropics (Davies et al., 2013; Kumar et al., 2015).

Previous studies of RCE have identified the strongest convective updrafts within the distribution as being those most sensitive to instability of the large-scale thermodynamic environment (Singh & O'Gorman, 2015). In our simulations, however, these extreme updrafts, represented by the 99.99th percentile of the vertical velocity distribution, have similar magnitudes irrespective of the forcing strength. Thus, under large-scale forcing, the magnitude of the strongest updrafts does not appear to be a simple function of instability, as

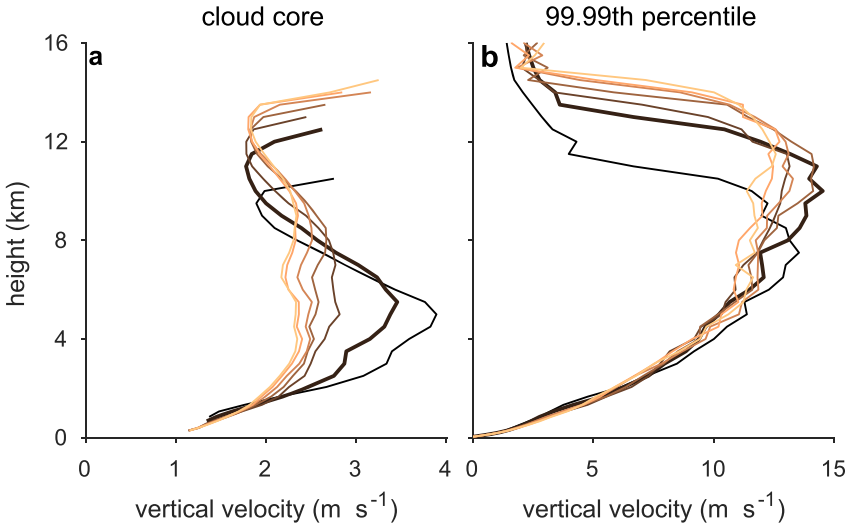

Figure 7. Profiles of vertical velocity given by (a) the mean value in cloud cores, defined as cloudy gridpoints in which $w > 1$ m s^{-1}, and (b) the 99.99th percentile at each level for CRM simulations with SST = 300 K and large-scale forcing magnitudes of $w_0 = -0.5$ (black), 0, 1, 2, 3, 4, and 5 (orange) cm s^{-1} (thick line gives RCE case).

measured by, for example, the CAPE. Clearly, further work is required to understand how large-scale forcing and the thermodynamic environment each affect the extreme tails of the vertical velocity distribution. We note, however, that the insensitivity of extreme updraft speeds to large-scale forcing is broadly in line with observational evidence that shows that the strongest thunderstorms (Zipser et al., 2006) and the highest frequency of lightning strikes (Singh et al., 2017) occur in the convective margins, rather in regions of highest mean precipitation.

4. Conclusions

We have developed a simple steady-state bulk-plume model for the temperature and relative humidity profiles of the atmosphere under the influence of an imposed large-scale flow. The model predicts an increase in relative humidity and stability of the troposphere with increasing large-scale upward motion, and these results are reproduced in simulations with a CRM forced with large-scale vertical velocity profiles. With some further simplifying assumptions, the model may be used to construct a one-parameter family of curves relating the nondimensionalized mean precipitation rate to the tropospheric relative humidity.

Despite its simplicity, the bulk-plume model qualitatively captures some important aspects of the relationships between humidity, instability, and precipitation in the tropical atmosphere. In particular, the model predicts a rapid increase of precipitation with tropospheric humidity qualitatively consistent with that seen in multiple observational analyses at multiple temporal scales (Bretherton et al., 2004; Peters & Neelin, 2006; Rushley et al., 2018; Singh et al., 2017). At short time scales, this relationship has been interpreted in terms of the sensitivity of convective mass fluxes to tropospheric humidity (e.g., Sahany et al., 2012). The bulk-plume model, however, considers the steady-state response of the atmosphere to a given large-scale forcing. Under such conditions, the precipitation rate is controlled by the requirement that latent heating roughly balance the adiabatic cooling that occurs as a result of the imposed large-scale vertical velocity, and the precipitation rate is not directly sensitive to the environmental humidity profile. Instead, the precipitation-humidity relationship is driven by the effect of convective detrainment on the environmental humidity. This is consistent with the recent conceptual model of Emanuel (2019), in which a strong relationship between precipitation and humidity is produced independently of a direct sensitivity of convection to environmental humidity. The steady-state constraints described above are not relevant to the onset of precipitation at convective time scales (e.g., Schiro et al., 2018), but they may be relevant for the climatology and for circulations that evolve over sufficiently long time scales (intraseasonal and greater).

Both the CRM simulations and the bulk-plume model predict that the mean lapse rate becomes more stable with increasing vertical motion. For the bulk-plume model, this result is based on the assumption of small cloud buoyancy (Bretherton & Park, 2008; Singh & O'Gorman, 2013), which leads to the most unstable

lapse rates occurring under large-scale descent when the environmental relative humidity is the lowest. The importance of relative humidity in setting the lapse rate has been recognized in a growing body of work examining idealized simulations of RCE (Romps, 2016; Seeley & Romps, 2015; Singh & O'Gorman, 2013; Singh & O'Gorman, 2015), and similar arguments have been applied to convective regions of the tropics to explain the fact that CAPE is the largest and lightning is the most frequent when the free troposphere is relatively dry (Singh et al., 2017). It should be noted, however, that while the vertical velocity in cloud cores increases with increasing instability in our simulations, the strongest updrafts (as represented by the 99.99th percentile of the vertical velocity distribution) are relatively insensitive to changes in the large-scale thermodynamic environment.

While the bulk-plume model derived here presents a useful framework for understanding the relationships between humidity, instability, and precipitation in both observations and general circulation models, it has a number of limitations. Most importantly, as mentioned above, the model is constructed in steady state, and it therefore is only applicable to large-scale circulations that evolve slowly compared to the timescale over which the atmosphere is moistened by convection. The equilibration of our CRM simulations suggests that this time scale is of the order of 10 days. Additionally, while a steady-state bulk-plume-based approach is reasonable in atmospheric columns that are continuously moistened by convection (Folkins et al., 2002; Minschwaner & Dessler, 2004; Romps, 2014), such an approach does not account for regions in which there is no convection. With no convective moistening, air parcels conserve their mixing ratio as they are advected, both horizontally and vertically, by the large-scale flow, and this advective transport is key to recovering the observed relative humidity distribution over the tropics as a whole (e.g., Sherwood, 1996; Galewsky et al., 2005; Pierrehumbert et al., 2007; Sherwood et al., 2010; O'Gorman et al., 2011).

The bulk-plume model must also necessarily include only a crude representation of precipitation reevaporation. In this work we assumed that the detrainment of condensate from clouds is proportional to the detrainment of water vapor at the same level, and we assumed that this detrained condensate evaporates at the level at which it is detrained or precipitates directly to the surface. These assumptions are unlikely to be satisfied in our simulations or in the tropical atmosphere, and their inaccuracy may account for some of the differences between the predictions of the bulk-plume model and the simulated environmental relative humidity profiles. In particular, the bulk-plume model is highly sensitive to the evaporation parameterization under large-scale descent, and further work is required to incorporate reevaporation into simple bulk-plume models in a physically realistic way.

Finally, the bulk-plume model cannot easily account for the effects of different types of convective organization on the large-scale thermodynamic properties of the atmosphere. In our CRM simulations, small changes to the implementation of the forcing led to important changes in the organizational structure of convection within the domain and ultimately changes to the mean thermodynamic profiles. Similar spontaneous convective organization has been studied in detail in simulations of RCE (e.g., Bretherton et al., 2004; Muller & Held, 2012; Wing & Emanuel, 2014). Understanding the mechanisms leading to organization under large-scale forcing is particularly important since the tropical atmosphere is not typically close to RCE on scales of a few hundred km (Jakob et al., 2019).

Appendix A : Effect of Large-Scale Horizontal Advection of Humidity

Here we explore the effect of large-scale horizontal advection on the relative humidity predicted by the bulk-plume model. We begin with the environmental humidity budget (6), which we write as

$$-M_d \frac{\partial q_{ve}}{\partial z} + (q_{ve} - q_x)\frac{\partial M_{\text{net}}}{\partial z} = M_u \delta_T (q^*_{vc} - q_{ve}),$$

where we have included the parameterization for evaporation (18) by replacing δ with δ_T on the right-hand side. Dividing by $M_u q^*_{vc}$, assuming $\mathcal{R} = q_{ve}/q^*_{vc}$ and neglecting vertical variations in relative humidity, we have

$$r\mathcal{R}\gamma + \left(\mathcal{R} - \frac{q_x}{q^*_{vc}}\right)\frac{1}{M_u}\frac{\partial M_{\text{net}}}{\partial z} = \delta_T(1 - \mathcal{R}).$$

Large-scale upward motion profiles of the form (22) imply convergence in the lower troposphere, and in this region we follow Raymond and Zeng (2005) and take q_x to be the humidity profile of the RCE state.

Furthermore, we assume that the saturation specific humidity remains similar to its RCE value so that $q_x/q^*_{vc} \approx \mathcal{R}_{\rm RCE}$. Expressing the plume mass flux in terms of the net mass flux and the ratio r, we may write

$$r\mathcal{R}\gamma + \left(\mathcal{R} - \mathcal{R}_{\rm RCE}\right)(1-r)\frac{1}{M_{\rm net}}\frac{\partial M_{\rm net}}{\partial z} = \delta_T(1-\mathcal{R}),$$

valid for regions of large-scale convergence. To estimate the second term on the left-hand side, we take the forcing to be of the form (22), and we take a mean value for the derivative of the net mass flux over the lower troposphere so that

$$\frac{1}{M_{\rm net}}\frac{\partial M_{\rm net}}{\partial z} \approx \frac{4}{H}.$$

Combining the previous two equations, we may derive a diagnostic for the environmental relative humidity

$$\mathcal{R} = \frac{\delta_T + 4(1-r)H^{-1}\mathcal{R}_{\rm RCE}}{\delta_T + r\gamma + 4(1-r)H^{-1}}.$$

Following the same steps as in section 2.3, we may also derive a relationship between precipitation and relative humidity in the presence of large-scale horizontal advection given by

$$\frac{P}{P_{\rm RCE}} = \frac{\mathcal{R} - B(\mathcal{R} - \mathcal{R}_{\rm RCE})}{\mathcal{R}_{\rm RCE} - B(\mathcal{R} - \mathcal{R}_{\rm RCE})\frac{1-\mathcal{R}_{\rm RCE}}{1-\mathcal{R}}}\left[1 + \frac{\mathcal{R} - \mathcal{R}_{\rm RCE}}{(1-\mathcal{R})(1-\mathcal{R}_{\rm RCE})}\right], \tag{A1}$$

where we have assumed that the vertical integral of $s_{\rm net}$ is dominated by the lower troposphere (where the large-scale flow is convergent), and we have defined the nondimensional parameter $B = 4(\gamma H)^{-1}$ and neglected its vertical variations.

As for the no-horizontal-advection case, (A1) predicts that the precipitation rate increases rapidly with the environmental humidity. But when large-scale horizontal advection is included, the increase in precipitation is even more rapid and the precipitation rate asymptotes to infinity at a maximum relative humidity given by

$$\mathcal{R}_{max} = \frac{1 + B(1-\mathcal{R}_{\rm RCE})}{1 + B\frac{(1-\mathcal{R}_{\rm RCE})}{\mathcal{R}_{\rm RCE}}}. \tag{A2}$$

For reasonable values of $H = 12.5$ km and $\gamma^{-1} = 4$ km (giving $B = 1.28$), the effect of large-scale horizontal advection on the precipitation-relative humidity relationship is relatively small. The difference in the relationships (15) and (A1) is comparable in magnitude to the difference in the precipitation-relative humidity relationship for simulations at different surface temperatures (Figure 1).

Appendix B : Effect of Evaporation on Precipitation-Humidity Relationship

Here we determine how environmental evaporation affects the precipitation-relative humidity relationship predicted by the bulk-plume model. Consider the dry static energy budget of the environment, which may be written

$$M_d\frac{\partial s_e}{\partial z} = Q + \mu\delta L_v q^*_{vc}(1-\mathcal{R})M_u, \tag{B1}$$

where s is the dry static energy, Q is the radiative cooling rate, and the last term on the right-hand side represents evaporative cooling in the environment. Assuming that the lapse rate is roughly moist adiabatic and that $T_c \approx T_e$, we have that

$$\frac{\partial s_e}{\partial z} \approx -L_v\frac{\partial q^*_{vc}}{\partial z} = L_v\gamma q^*_{vc}.$$

Substituting this approximation into (B1) and rearranging gives

$$\left[1-\frac{\mu\delta}{r\gamma}(1-\mathcal{R})\right] rM_u = \frac{Q}{L_v q_{vc}^* \gamma},$$

where we have used $M_d = rM_u$. From (19), we have that $\frac{\delta_T}{r\gamma} = \frac{\mathcal{R}}{1-\mathcal{R}}$, and we may therefore write

$$\left[1-\frac{\mu}{1+\mu}\mathcal{R}\right] rM_u = \frac{Q}{L_v q_{vc}^* \gamma}.$$

Assuming that Q and $q_{vc}^*\gamma$ do not vary as the cloud mass flux varies, the right-hand side of the above equation is constant and equal to its value in RCE. We therefore have that

$$\left[1-\frac{\mu}{1+\mu}\mathcal{R}\right] rM_u = \left[1-\frac{\mu}{1+\mu}\mathcal{R}_{\mathrm{RCE}}\right] M_{\mathrm{RCE}}.$$

Finally, after some rearrangement, we have

$$M_u = \frac{M_{\mathrm{RCE}}}{r}\left[\frac{1+\mu(1-\mathcal{R}_{\mathrm{RCE}})}{1+\mu(1-\mathcal{R})}\right].$$

Substituting the above equation into (20) and following the same procedure as in section 2.3 gives the following relationship between the precipitation rate and the relative humidity

$$\frac{P}{P_{\mathrm{RCE}}} = \frac{\mathcal{R}}{\mathcal{R}_{\mathrm{RCE}}}\left[1+\frac{\mathcal{R}-\mathcal{R}_{\mathrm{RCE}}}{(1-\mathcal{R})(1-\mathcal{R}_{\mathrm{RCE}})}\right]\left[\frac{1+\mu(1-\mathcal{R}_{\mathrm{RCE}})}{1+\mu(1-\mathcal{R})}\right]. \tag{B2}$$

The above equation is plotted on Figure 1 for the case $\mu = 2$. The effect of evaporation in the environment is small for large-scale descent and weak ascent, but it acts to increase the precipitation rate for a given relative humidity when the large-scale ascent is strong. Physically, this is because an increased descent rate is required to balance evaporative cooling in the environment compared to the no-evaporation case. This higher descent rate is associated with stronger subsidence drying in the environment, decreasing the relative humidity for a given precipitation rate. Since the evaporation scales with the mass flux, this effect becomes larger with increasing precipitation rate.

Appendix C : Solution of the Bulk-Plume Model

We solve the bulk-plume model by constructing an explicit equation for the temperature lapse rate using a similar method to Romps (2014). We first combine (12), (13), and (19) to derive a quadratic equation for γ given by

$$\left(\gamma-\gamma_m\right)\left(r\gamma+\delta_T\right)-\varepsilon rQ\gamma = 0, \tag{C1}$$

where

$$Q = \frac{L_v^2 q_{ve}^*}{q_{ve}^* L_v^2 + c_p R_v T_e^2}$$

and γ_m is the fractional humidity gradient along a moist adiabat, given by

$$\gamma_m = -\left(\frac{\partial \ln q_v^*}{\partial z}\right)_{h^*} = \frac{g}{c_p T}\left(\frac{\frac{L_v}{R_v T}-\frac{c_p}{R_d}}{1+\frac{L_v^2 q_v^*}{c_p R_v T^2}}\right).$$

Expressing (C1) in terms of $(\gamma-\gamma_m)$, solving the resultant quadratic, and expressing the result in terms of the lapse rate, we may write

$$\Gamma = \Gamma_m + \frac{R_v T_e^2}{2L_v}\left\{\left[\left(\gamma_m + \frac{\delta_T}{r} - \varepsilon Q\right)^2 + 4\varepsilon Q\gamma_m\right]^{1/2} - (\gamma_m + \frac{\delta_T}{r} - \varepsilon Q)\right\}, \tag{C2}$$

where Γ_m is the moist adiabatic lapse rate

$$\Gamma_m = -\left(\frac{\partial T}{\partial z}\right)_{h^*} = \frac{g}{c_p}\left(\frac{1 + \frac{L_v q_v^*}{R_d T}}{1 + \frac{L_v^2 q_v^*}{c_p R_v T^2}}\right),$$

and we have taken the root that ensures that $\Gamma \to \Gamma_m$ as $\varepsilon \to 0$.

We integrate (C2) in combination with the equation for hydrostatic balance

$$\frac{\partial \ln p}{\partial z} = -\frac{g}{R_d T_e}, \tag{C3}$$

upward from cloud base ($z_b = 1,062$ m) given the profile of cloud mass flux M_u, the domain-mean vertical velocity $\overline{w}$, the entrainment rate ε, and the evaporation parameter μ. We take as an initial condition the mean temperature and pressure values in the corresponding simulation at $z = z_b$, and the integration is completed using forward differences with a step size of 100 m up to the level at which the cloud mass flux decreases to zero. At each step in the integration, the detrainment rate is calculated using (1), the ratio r is calculated using (2) and (3), and the right-hand sides of (C2) and (C3) are then evaluated using a thermodynamic formulation consistent with SAM. To account for the effects of freezing, L_v is taken as the latent heat of vaporization for $T > 273.15$ K and the latent heat of sublimation otherwise. Finally, given the profile of temperature and pressure, the relative humidity is calculated based on (13) and (19).

Acknowledgments
We thank D. Romps, D. Neelin, and an anonymous reviewer for detailed and constructive reviews. The SAM model was provided by M. Khairoutdinov; source code for this model is available upon registration (http://rossby.msrc.sunysb.edu/~marat/SAM.html). Model output data, code for the plume model, and analysis scripts to produce all figures are available through Monash.figshare (DOI: https://doi.org/10.26180/5db26bbd7ff51). The authors acknowledge support from the Australian Research Council through the Centre of Excellence for Climate Extremes (CE170100023; C. J., R. A. W., and M. S.) and DECRA award (DE190100866; M. S.). R. A. W. was also supported by the National Environmental Science Program through the Earth Systems and Climate Change Hub. Computational resources and services from the National Computational Infrastructure (NCI), which is supported by the Australian Government, are gratefully acknowledged.

References

Ahmed, F., & Neelin, J. D. (2018). Reverse engineering the tropical precipitation-buoyancy relationship. *Journal of the Atmospheric Sciences*, *75*(5), 1587–1608. https://doi.org/10.1175/JAS-D-17-0333.1

Bretherton, C. S., Blossey, P. N., & Khairoutdinov, M. (2005). An energy-balance analysis of deep convective self-aggregation above uniform SST. *Journal of the Atmospheric Sciences*, *62*(12), 4273–4292. https://doi.org/10.1175/JAS3614.1

Bretherton, C. S., & Park, S. (2008). A new bulk shallow-cumulus model and implications for penetrative entrainment feedback on updraft buoyancy. *Journal of the Atmospheric Sciences*, *65*(7), 2174–2193. https://doi.org/10.1175/2007JAS2242.1

Bretherton, C. S., Peters, M. E., & Back, L. E. (2004). Relationships between water vapor path and precipitation over the tropical oceans. *Journal of Climate*, *17*(7), 1517–1528. https://doi.org/10.1175/1520-0442(2004)017<1517:RBWVPA>2.0.CO;2

Bryan, G. H., & Fritsch, J. M. (2002). A benchmark simulation for moist nonhydrostatic numerical models. *Monthly Weather Review*, *130*(12), 2917–2928. https://doi.org/10.1175/1520-0493(2002)130<2917:ABSFMN>2.0.CO;2

Clough, S. A., Shephard, M. W., Mlawer, E. J., Delamere, J. S., Iacono, M. J., Cady-Pereira, K., et al. (2005). Atmospheric radiative transfer modeling: A summary of the AER codes. *Journal of Quantitative Spectroscopy & Radiative Transfer*, *91*(2), 233–244. https://doi.org/10.1016/j.jqsrt.2004.05.058

Davies, L., Jakob, C., May, P., Kumar, V. V., & Xie, S. (2013). Relationships between the large-scale atmosphere and the small-scale convective state for Darwin, Australia. *Journal of Geophysical Research: Atmospheres*, *118*, 11,534–11,545. https://doi.org/10.1002/jgrd.50645

Derbyshire, S. H., Beau, I., Bechtold, P., Grandpeix, J.-Y., Piriou, J.-M., Re-delsperger, J.-L., & Soares, P. M. M. (2004). Sensitivity of moist convection to environmental humidity. *Quarterly Journal of the Royal Meteorological Society*, *130*(604), 3055–3079. https://doi.org/10.1256/qj.03.130

Emanuel, K. (2019). Inferences from simple models of slow, convectively coupled processes. *Journal of the Atmospheric Sciences*, *76*(1), 195–208. https://doi.org/10.1175/JAS-D-18-0090.1

Emanuel, K. A., Neelin, J. D., & Bretherton, C. S. (1994). On large-scale circulations in convecting atmospheres. *Quarterly Journal of the Royal Meteorological Society*, *120*(519), 1111–1143. https://doi.org/10.1002/qj.49712051902

Folkins, I., Kelly, K. K., & Weinstock, E. M. (2002). A simple explanation for the increase in relative humidity between 11 and 14 km in the tropics. *Journal of Geophysical Research*, *107*(D23), ACL 26-1–ACL 26-7. https://doi.org/10.1029/2002JD002185

Galewsky, J., Sobel, A., & Held, I. (2005). Diagnosis of subtropical humidity dynamics using tracers of last saturation. *Journal of the Atmospheric Sciences*, *62*(9), 3353–3367. https://doi.org/10.1175/JAS3533.1

Hamada, A., Takayabu, Y. N., Liu, C., & Zipser, E. J. (2015). Weak linkage between the heaviest rainfall and tallest storms. *Nature Communications*, *6*(1), 6213. https://doi.org/10.1038/ncomms7213

Holloway, C. E., & Neelin, J. D. (2009). Moisture vertical structure, column water vapor, and tropical deep convection. *Journal of the Atmospheric Sciences*, *66*(6), 1665–1683. https://doi.org/10.1175/2008JAS2806.1

Jakob, C., Singh, M. S., & Jungandreas, L. (2019). Radiative convective equilibrium and organised convection: An observational perspective. *Journal of Geophysical Research: Atmospheres*, *124*, 5418–5430. https://doi.org/10.1029/2018JD030092

Khairoutdinov, M. F., & Randall, D. A. (2003). Cloud resolving modeling of the ARM summer 1997 IOP: Model formulation, results, uncertainties, and sensitivities. *Journal of the Atmospheric Sciences*, *60*(4), 607–625. https://doi.org/10.1175/1520-0469(2003)060<0607:CRMOTA>2.0.CO;2

Kumar, V. V., Jakob, C., Protat, A., Williams, C. R., & May, P. T. (2015). Mass-flux characteristics of tropical cumulus clouds from wind profiler observations at Darwin, Australia. *Journal of the Atmospheric Sciences*, *72*(5), 1837–1855. https://doi.org/10.1175/JAS-D-14-0259.1

Kuo, Y.-H., Neelin, J. D., & Mechoso, C. R. (2017). Tropical convective transition statistics and causality in the water vapor-precipitation relation. *Journal of the Atmospheric Sciences*, *74*(3), 915–931. https://doi.org/10.1175/JAS-D-16-0182.1

Kuo, Y.-H., Schiro, K. A., & Neelin, J. D. (2018). Convective transition statistics over tropical oceans for climate model diagnostics: Observational baseline. *Journal of the Atmospheric Sciences*, *75*(5), 1553–1570. https://doi.org/10.1175/JAS-D-17-0287.1

Minschwaner, K., & Dessler, A. E. (2004). Water vapor feedback in the tropical upper troposphere: Model results and observations. *Journal of Climate*, *17*(6), 1272–1282. https://doi.org/10.1175/1520-0442(2004)017<1272:WVFITT>2.0.CO;2

Muller, C. J., Back, L. E., O'Gorman, P. A., & Emanuel, K. A. (2009). A model for the relationship between tropical precipitation and column water vapor. *Geophysical Research Letters*, *36*, L16804. https://doi.org/10.1029/2009GL039667

Muller, C. J., & Held, I. M. (2012). Detailed investigation of the self-aggregation of convection in cloud-resolving simulations. *Journal of the Atmospheric Sciences*, *69*(8), 2551–2565. https://doi.org/10.1175/JAS-D-11-0257.1

Neelin, J. D., & Held, I. M. (1987). Modeling tropical convergence based on the moist static energy budget. *Monthly Weather Review*, *115*(1), 3–12. https://doi.org/10.1175/1520-0493(1987)115<0003:MTCBOT>2.0.CO;2

O'Gorman, P. A., Lamquin, N., Schneider, T., & Singh, M. S. (2011). The relative humidity in an isentropic advection-condensation model: Limited poleward influence and properties of subtropical minima. *Journal of the Atmospheric Sciences*, *68*(12), 3079–3093. https://doi.org/10.1175/JAS-D-11-067.1

Paluch, I. R. (1979). The entrainment mechanism in Colorado cumuli. *Journal of the Atmospheric Sciences*, *36*(12), 2467–2478. https://doi.org/10.1175/1520-0469(1979)036<2467:TEMICC>2.0.CO;2

Peters, O., & Neelin, J. D. (2006). Critical phenomena in atmospheric precipitation. *Nature Physics*, *2*(6), 393–396. https://doi.org/10.1038/nphys314

Pierrehumbert, R., Brogniez, H., & Roca, R. (2007). On the relative humidity of the atmosphere. In A. H. Sobel & T. Schneider (Eds.), *The general circulation of the atmosphere* (pp. 143–185). New Jersey, USA: Princeton University Press.

Raymond, D. J., & Zeng, X. (2005). Modelling tropical atmospheric convection in the context of the weak temperature gradient approximation. *Quarterly Journal of the Royal Meteorological Society*, *131*(608), 1301–1320. https://doi.org/10.1256/qj.03.97

Romps, D. M. (2014). An analytical model for tropical relative humidity. *Journal of Climate*, *27*(19), 7432–7449. https://doi.org/10.1175/JCLI-D-14-00255.1

Romps, D. M. (2016). Clausius-Clapeyron scaling of CAPE from analytical solutions to RCE. *Journal of the Atmospheric Sciences*, *73*(9), 3719–3737. https://doi.org/10.1175/JAS-D-15-0327.1

Rushley, S. S., Kim, D., Bretherton, C. S., & Ahn, M.-S. (2018). Reexamining the nonlinear moisture-precipitation relationship over the tropical oceans. *Geophysical Research Letters*, *45*(2), 1133–1140. https://doi.org/10.1002/2017GL076296

Sahany, S., Neelin, J. D., Hales, K., & Neale, R. B. (2012). Temperature-moisture dependence of the deep convective transition as a constraint on entrainment in climate models. *Journal of the Atmospheric Sciences*, *69*(4), 1340–1358. https://doi.org/10.1175/JAS-D-11-0164.1

Schiro, K. A., Ahmed, F., Giangrande, S. E., & Neelin, J. D. (2018). GoAmazon2014/5 campaign points to deep-inflow approach to deep convection across scales. *Proceedings of the National Academy of Sciences of the United States of America*, *115*(18), 4577–4582. https://doi.org/10.1073/pnas.1719842115

Schiro, K. A., Neelin, J. D., Adams, D. K., & Lintner, B. R. (2016). Deep convection and column water vapor over tropical land versus tropical ocean: A comparison between the Amazon and the Tropical Western Pacific. *Journal of the Atmospheric Sciences*, *73*(10), 4043–4063. https://doi.org/10.1175/JAS-D-16-0119.1

Seeley, J. T., & Romps, D. M. (2015). Why does tropical convective available potential energy (CAPE) increase with warming? *Geophysical Research Letters*, *42*, 10,429–10,437. https://doi.org/10.1002/2015GL066199

Sherwood, S. C. (1996). Maintenance of the free-tropospheric tropical water vapor distribution. Part II: Simulation by large-scale advection. *Journal of Climate*, *9*(11), 2919–2934. https://doi.org/10.1175/1520-0442(1996)009<2919:MOTFTT>2.0.CO;2

Sherwood, S. C., Roca, R., Weckwerth, T. M., & Andronova, N. G. (2010). Tropospheric water vapor, convection, and climate. *Reviews of Geophysics*, *48*, RG2001. https://doi.org/10.1029/2009RG000301

Singh, M. S., Kuang, Z., Maloney, E. D., Hannah, W. M., & Wolding, B. O. (2017). Increasing potential for intense tropical and subtropical thunderstorms under global warming. *Proceedings of the National Academy of Sciences of the United States of America*, *114*(44), 11,657–11,662. https://doi.org/10.1073/pnas.1707603114

Singh, M. S., & O'Gorman, P. A. (2013). Influence of entrainment on the thermal stratification in simulations of radiative-convective equilibrium. *Geophysical Research Letters*, *40*, 4398–4403. https://doi.org/10.1002/grl.50796

Singh, M. S., & O'Gorman, P. A. (2015). Increases in moist-convective updraught velocities with warming in radiative-convective equilibrium. *Quarterly Journal of the Royal Meteorological Society*, *141*(692), 2828–2838. https://doi.org/10.1002/qj.2567

Thayer-Calder, K., & Randall, D. A. (2009). The role of convective moistening in the Madden-Julian Oscillation. *Journal of the Atmospheric Sciences*, *66*(11), 3297–3312. https://doi.org/10.1175/2009JAS3081.1

Tiedtke, M. (1989). A comprehensive mass flux scheme for cumulus parameterization in large-scale models. *Monthly Weather Review*, *117*(8), 1779–1800. https://doi.org/10.1175/1520-0442(1996)009<2919:MOTFTT>2.0.CO;2

Virman, M., Bister, M., Sinclair, V. A., Jarvinen, H., & Raisanen, J. (2018). A new mechanism for the dependence of tropical convection on free-tropospheric humidity. *Geophysical Research Letters*, *45*(5), 2516–2523. https://doi.org/10.1002/2018GL077032

Wing, A. A., & Emanuel, K. A. (2014). Physical mechanisms controlling self-aggregation of convection in idealized numerical modeling simulations. *Journal of Advances in Modeling Earth Systems*, *6*, 59–74. https://doi.org/10.1002/2013MS000269

Wing, A. A., Reed, K. A., Satoh, M., Stevens, B., Bony, S., & Ohno, T. (2018). Radiative-convective equilibrium model intercomparison project. *Geoscientific Model Development*, *11*(2), 793–813. https://doi.org/10.5194/gmd-11-793-2018

Xu, K.-M., & Emanuel, K. A. (1989). Is the tropical atmosphere conditionally unstable? *Monthly Weather Review*, *117*(7), 1471–1479. https://doi.org/10.1175/1520-0493(1989)117<1471:ITTACU>2.0.CO;2

Zipser, E. J., Cecil, D. J., Liu, C., Nesbitt, S. W., & Yorty, D. P. (2006). Where are the most intense thunderstorms on Earth? *Bulletin of the American Meteorological Society*, *87*(8), 1057–1072. https://doi.org/10.1175/BAMS-87-8-1057